Atmos. Chem. Phys. Discuss., doi:10.5194/acp-2017-148, 2017
Manuscript under review for journal Atmos. Chem. Phys.
Discussion started: 23 February 2017


Atmospheric Chemistry and Physics Discussions

# Aerosol Effects on the Development of Cumulus Clouds over the Tibetan Plateau

Xu Zhou[1,5], Naifang Bei[2], Hongli Liu[3], Junji Cao[1], Li Xing[1], Wenfang Lei[4], Luisa T. Molina[4], and Guohui Li[1*]

[1]Key Lab of Aerosol Chemistry and Physics, SKLLQG, Institute of Earth Environment, Chinese Academy of Sciences, Xi'an, China
[2]School of Human Settlements and Civil Engineering, Xi'an Jiaotong University, Xi'an, Shaanxi, China
[3]State Key Laboratory of Severe Weather, Chinese Academy of Meteorological Sciences, Beijing, China
[4]Molina Center for Energy and the Environment, La Jolla, CA, USA
[5]University of Chinese Academy of Science, Beijing, China
[*]Correspondence to: Guohui Li (ligh@ieecas.cn)

**Abstract.** The aerosol-cloud interaction over the Tibetan Plateau has been investigated using a cloud-resolving weather research and forecasting model with a two-moment bulk microphysical scheme including aerosol effects on cloud condensation nuclei and ice nuclei. Two types of cumulus clouds with a similar convective available potential energy, occurring over the Tibetan Plateau (Cu-TP) and North China Plain (Cu-NCP) in August 2014, are simulated to explore the response of convective clouds to aerosols. A set of aerosol profiles is used in the simulations, with the surface aerosol number concentration varying from 20 to 9000 $cm^{-3}$ and the sulfate mass concentration varying from 0.02 to 9.0 μg $cm^{-3}$. Increasing aerosol concentrations generally enhances the cloud core updraft and maximum updraft, intensifying convections in Cu-TP and Cu-NCP. However, the core updraft is much stronger in Cu-TP than Cu-NCP, because of the early occurrence of the glaciation process in Cu-TP that is triggered at an elevation above 4000 m. The precipitation increases steadily with aerosol concentrations in Cu-NCP, caused by the suppression of the warm rain but efficient mix-phased precipitation due to the reduced cloud droplet size. The precipitation in Cu-TP also increases with aerosol concentrations, but the precipitation enhancement is not substantial compared to that in Cu-NCP with high aerosol concentrations. The aerosol-induced intensification of convections in Cu-TP not only facilitates the precipitation, but also transports more ice-phase hydrometeors into the upper troposphere to decrease the precipitation efficiency. Considering the very clean atmosphere over the Tibetan Plateau, elevated aerosol concentrations can remarkably enhance convections due to its specific topography, which not only warms the middle troposphere to influence the Asian summer monsoon, but also delivers hydrometeors into the upper troposphere to allow more water vapor to travel into the lower stratosphere.

Atmos. Chem. Phys. Discuss., doi:10.5194/acp-2017-148, 2017
Manuscript under review for journal Atmos. Chem. Phys.
Discussion started: 23 February 2017


Atmospheric Chemistry and Physics Discussions

## 1 Introduction

Atmospheric aerosols, formed naturally and anthropogenically, influence the radiative energy budget of the Earth-atmosphere system in many ways. They scatter or absorb a fraction of the incoming solar radiation to cool or warm the atmosphere, decreasing surface temperature and altering atmospheric stability (e.g., Ackerman, 1977; Jacobson, 2002). They also serve as cloud condensation nuclei (CCN) and ice nuclei (IN), modifying optical properties and lifetime of clouds (e.g., Penner et al., 2001; Zhang et al., 2007). The aerosol indirect effect, generally referred to as the aerosol impact on cloud reflective properties and lifetime (Twomey, 1977; Houghton, 2001), has constituted the one of the largest uncertainties in climate prediction (IPCC, 2013). In addition, the aerosol effects on precipitation have been regarded as an important but poorly understood process that could have major implications to climate and water supplies (Levin and Cotton, 2007).

For a given amount of condensable water vapor, elevated aerosol concentrations increase the number of cloud droplets and reduce their sizes, enhancing not only the reflective properties but also the lifetime of clouds through suppressing warm rain processes (Twomey, 1977; Albrecht, 1989). Accumulative observational and modeling evidence has shown that reduced cloud droplet size, due to increasing CCN, inhibits collision and coalescence processes, suppressing warm rain and delaying the onset of precipitation. Therefore, more droplets are further allowed to be transported above the 0°C isotherm, triggering the efficient mixed-phase process to release more latent heat and intensify the convection (e.g. Rosenfeld and Lensky, 1998; Rosenfeld and Woodley, 2000; Kaufman and Nakajima, 1993; Andreae et al., 2004; Kaufman et al., 2005; Fan et al., 2007; Khain et al., 2008; Koren et al., 2010; Li et al., 2013; Loftus and Cotton, 2014). However, recent studies have shown that an optimal aerosol loading exists to invigorate convection (Rosenfeld et al., 2008; Koren et al., 2014; Dagan et al., 2015). Additionally, the aerosol impacts on cloud

Atmos. Chem. Phys. Discuss., doi:10.5194/acp-2017-148, 2017
Manuscript under review for journal Atmos. Chem. Phys.
Discussion started: 23 February 2017




63 developments are also proposed to be dependent on the environmental conditions, such as
64 relative humidity and vertical wind shear (Tao et al., 2007; van den Heever et al., 2007; Lee
65 et al., 2008; Fan et al., 2009).

66 The observational and model-derived evidence on how aerosols influence rainfall
67 remains elusive due to the complexity of cloud processes, which are determined by intricate
68 thermodynamic, dynamical, and microphysical processes and their interactions (Hobbs, 1993;
69 Levin and Cotton, 2007; McComiskey and Feingold, 2012). Observations have demonstrated
70 that the aerosol effect on precipitation depends on both the type of aerosols and precipitating
71 environments. Rainfall reduction has been observed in polluted industrial and urban regions
72 in shallow clouds or clouds with the top temperature exceeding -10°C (e.g., Rosenfeld, 2000;
73 Ramanathan et al., 2001; Andreae et al., 2004; Yang et al., 2013). However, documented
74 rainfall increase has also been observed around heavily polluted coastal areas or over oceans
75 influenced by anthropogenic aerosols (e.g., Cerveny and Balling, 1998; Shepherd and Burian,
76 2003; Zhang et al., 2007; Li et al., 2008b; Koren et al., 2012, 2014). Model results tend to
77 support the argument that increasing aerosol concentrations enhances precipitation under a
78 moist, unstable atmosphere (e.g., Khain et al., 2005; Fan et al., 2007; Li et al., 2008a, 2009;
79 Fan et al., 2013).

80 The Tibetan Plateau (TP), located in the central eastern Eurasia and with an average
81 elevation of more than 4000 m, significantly affects the formation and variability of the Asian
82 summer monsoon through mechanical and thermal dynamical effects (Wu et al., 2007). Due
83 to its strong surface heating, the cumulus clouds are active over the TP and can be organized
84 to form convective systems, contributing substantially to the precipitation over TP and
85 adjacent areas. The TP is surrounded by several important natural and anthropogenic aerosol
86 sources, and the in-situ and satellite measurements have shown that anthropogenic aerosols
87 and dust have been lofted to the TP, directly influencing the regional climate (Engling et al.,

Atmos. Chem. Phys. Discuss., doi:10.5194/acp-2017-148, 2017
Manuscript under review for journal Atmos. Chem. Phys.
Discussion started: 23 February 2017




2011). Soot aerosols deposited on the TP glaciers have been confirmed to contribute significantly to observed glacier retreat (Xu et al., 2009). Absorbing aerosols over the TP have been proposed to directly affect monsoon rainfall through the elevated heat pump mechanism (Ding et al., 2008; Lau et al., 2008; D'Errico et al., 2015).

However, to date few studies have been performed to investigate the aerosol indirect effect or the aerosol-cloud interaction over the TP. In the present study, we report an investigation of the aerosol effect on the cumulus cloud development and precipitation over the TP. Two types of cumulus clouds occurring over the TP and the North China Plain (NCP) are simulated using a cloud-resolving weather research and forecasting model for comparisons. The model configuration is described in Section 2. The results and discussions are presented in Section 3, and summary and conclusions are given in Section 4.

## 2 Models and Design of Numerical Experiments

### 2.1 Model Configuration

A cloud-resolving weather research and forecasting (CR-WRF) model (Skamarock et al., 2004) is used in the study to simulate cumulus clouds. A two-moment bulk microphysical scheme developed by Li et al. (2008a) is utilized to account for the aerosol-cloud interactions in the simulations. The mass mixing ratio and number concentration of five hydrometeors are predicted in the bulk microphysical scheme, including cloud water, rain water, ice crystal, snow flake, and graupel. The gama function is used to represent the size distribution of the five hydrometeors. Detailed information is provided in Li et al. (2008a).

In order to consider the aerosol activation to CCN and IN, the CMAQ/models3 aerosol module (Binkowski and Roselle, 2003) is implemented into the CR-WRF model. Aerosols are simulated in the CMAQ using a modal approach assuming that particles are represented by three superimposed log-normal size distributions. The aerosol species, including sulfate,

Atmos. Chem. Phys. Discuss., doi:10.5194/acp-2017-148, 2017
Manuscript under review for journal Atmos. Chem. Phys.
Discussion started: 23 February 2017




nitrate, ammonium, organic and black carbon, and other unidentified species (dust-like) are predicted in the module.

For the CCN nucleation, the critical radius of dry aerosols is calculated from the *k*-Köhler theory developed by Petters and Kreidenweis (2007; 2008; 2013) using water supersaturation predicted by the CR-WRF model (Roger and Yau, 1989; Pruppacher and Klett, 1997). If the activated CCN radius is less than 0.03 μm, the mass of water condensation on CCN is calculated under the equilibrium assumption; otherwise, the mass of water condensing on CCN is calculated by $m_w = K\frac{4}{3}\pi r_a^3 \rho_w$ at zero supersaturation, where $3 < K < 8$ (Khain et al., 2000). Additionally, a novel, flexible approach, proposed by Philips et al. (2008, 2013) has been used to parameterize the ice heterogeneous nucleation within clouds. The method has empirically derived dependencies on the chemistry and surface area of multiple species of IN aerosols, mainly including dust, black and organic carbon aerosols. Three kinds of ice nucleation mechanisms are considered in the method, including contact, immersion, and condensation freezing.

### 2.2 Design of Numerical Experiments and Statistical Method in Data Analysis

The spatial resolution used in the cloud simulations is 1 km in the horizontal direction and about 250 m in the vertical direction. The model domain of 200 × 200 × 80 grid boxes along the x, y, and z directions, respectively, has been used to provide 200 km × 200 km horizontal and 20-km vertical coverage in this study. The simulations use the open boundary conditions under which variables of all horizontal gradients are zero at the lateral boundary.

Two types of cumulus clouds are simulated using the CR-WRF model. The cumulus cloud over the TP (hereafter referred to as Cu-TP) is initialized using the sounding data (87.08°E, 28.63°N, 4302 m a.s.l.) at 0800 UTC on August 24, 2014 (Figure 1a). The cumulus cloud over the NCP (hereafter referred to as Cu-NCP) is initialized using the sounding data (114.35°E, 37.17°N, 181 m a.s.l.) at 0800 UTC on August 12, 2014 (Figure 1b). The selected

Atmos. Chem. Phys. Discuss., doi:10.5194/acp-2017-148, 2017
Manuscript under review for journal Atmos. Chem. Phys.
Discussion started: 23 February 2017




sounding profiles over the TP and NCP reveal a moderate instability in the atmosphere, with similar convective available potential energy (CAPE) for comparison, i.e., 675 J $kg^{-1}$ for Cu-TP and 651 J $kg^{-1}$ for Cu-NCP. Although Cu-TP and Cu-NCP have the similar CAPE, the remarkable difference of the initialization elevation between Cu-TP and Cu-NCP causes their distinct development processes. The 0°C isotherm is generally at the level of around 5 km a.s.l. in the summer. Therefore, when an air parcel perturbed in the boundary layer ascend to form cloud, the rising distance to the 0°C isotherm is at most 1 km over the TP and at least 4 km over the NCP. Therefore, the occurrence of the efficient mixed phase process is much earlier for the cumulus cloud over the TP than the NCP, which substantially advances the development of the cloud over the TP.

The cumulus development is triggered by a warm bubble 15-km wide and a maximum temperature anomaly of 4°C at the height of 1.5 km a.g.l. (Li et al., 2008a) and the integration time is two hours. A set of 28 initial aerosol size distributions with the aerosol number concentration ranging from 20 to 9000 $cm^{-3}$ and the sulfate mass concentration ranging from 0.02 to 9.0 μg $cm^{-3}$ at the surface level are used. Other aerosol species are scaled using the measurement at the Nepal Climate Observatory-Pyramid (Decesari et al., 2010). These aerosol distributions are designated for environments ranging from very clean background air mass to polluted urban plumes over the TP and NCP. The aerosol concentration is assumed to decrease exponentially with the height in the model simulations (Li et al., 2008a). We have adopted several assumptions and simplifications for the processes associated with aerosols. In the simulations, only the accumulation mode of aerosols is used for the CCN and IN activation, and the aerosol spatial distributions are determined by the initial and boundary conditions, without consideration of chemistry, emissions, and release from cloud droplet evaporation or ice crystal sublimation.

Atmos. Chem. Phys. Discuss., doi:10.5194/acp-2017-148, 2017
Manuscript under review for journal Atmos. Chem. Phys.
Discussion started: 23 February 2017


Atmospheric Chemistry and Physics Discussions

In order to evaluate the overall response of simulated cumulus clouds to changes in aerosol concentrations, the population mean (p-mean) of a given variable over all qualified grid points and for a given integration interval is used in the study (Wang, 2005), defined as:

$$\bar{C}^p = \frac{1}{\sum_{t=T_1}^{T_2} N(t)} \sum_{t=T_1}^{T_2} \sum_{n>n_{min}}^{q>q_{min}} c(x,y,t)$$

where $c$ represents a given quantity. The calculation only applies to the grid points where both the mass concentration $q$ and number concentration $n$ of a hydrometeor or the summation of several hydrometeors exceed the given minima. The total number of the grid points at a given output time step $t$ is represented by $N(t)$. $T_1$ and $T_2$ are the start and end output time steps, respectively.

## 3. Results and Discussions

### 3.1 Response of Cloud Properties to Changes in Aerosol Concentrations

Figure 2a depicts the dependence of the p-mean of the cloud droplet number concentration (CDNC) on the surface-level aerosol number concentration ([*Na*]). Increasing [*Na*] provides more CCN to activate, and although more activated droplets compete for the available water vapor, the water vapor condensation efficiency is enhanced due to the increased bulk droplet surface area, accelerating the latent heat release and the updraft to provide more supersaturated water vapor. Therefore, the increasing CDNC is well consistent with increasing [*Na*] in Cu-TP and Cu-NCP, in good agreement with previous studies (e.g., Fan et al., 2007a, b; Li et al., 2008a). When the [*Na*] increases from about 20 $cm^{-3}$ to 9000 $cm^{-3}$, the p-mean of the CDNC increases from 0.56 $cm^{-3}$ to 218 $cm^{-3}$ for Cu-NCP. However, more aerosols are activated in Cu-TP compared to Cu-NCP, and the p-mean of the CDNC increases from 0.80 $cm^{-3}$ to 415 $cm^{-3}$ for Cu-TP. Although the CAPE is similar for Cu-TP and Cu-NCP, the p-mean of CDNC in Cu-TP is higher than that in Cu-NCP with the same [*Na*].

Atmos. Chem. Phys. Discuss., doi:10.5194/acp-2017-148, 2017
Manuscript under review for journal Atmos. Chem. Phys.
Discussion started: 23 February 2017


Atmospheric Chemistry and Physics Discussions

With the [*Na*] increasing from 20 to 9000 $cm^{-3}$, the effective radius of cloud droplet ($R_{eff}$) in Cu-TP is reduced from about 18.5 to 4 .1 μm, and the $R_{eff}$ in Cu-NCP is also consistently reduced from 14.3 to 6.6 μm (Figure 2b). Interestingly, when the [*Na*] is less than about 240 $cm^{-3}$, the $R_{eff}$ in Cu-TP is larger than that in Cu-NCP with the same [*Na*], although the CDNC in Cu-TP is higher than that in Cu-NCP, showing more cloud water condensed in Cu-TP. Figure 3a presents the dependence of the cloud water content (CWC) on the [*Na*] in Cu-TP and Cu-NCP, showing that the CWC increases with increasing [*Na*]. This positive relationship is caused by the combined effects of the increase in CDNC and the decrease in $R_{eff}$, which inhibit the collision/coalescence of cloud droplets and also enhance the water vapor condensation efficiency and the updraft to generate more available condensable water vapor. The CWC in Cu-TP is higher than that in Cu-NCP for the same [*Na*], due to higher CDNC and likely stronger updrafts in Cu-TP. The Cu-TP is triggered at an elevation of more than 4000 m a.s.l. Therefore, considering that the 0°C isotherm is at the level of around 5000 m a.s.l., the cloud water formed in the cumulus tends to be transported above the 0°C isotherm to become supercooled, initiating the efficient mixed phase process to release more latent heat and enhance the updraft. Therefor, there exists more supercooled cloud water in Cu-TP than Cu-NCP when [*Na*] are same (Figure 3b).

Figure 4 provides the vertical profiles of the hydrometeors mass concentrations (summed over the horizontal domain and then averaged during the simulation period) under three aerosol scenarios: a very low [*Na*] of 90 $cm^{-3}$, a low [*Na*] of 900 $cm^{-3}$, and a high [*Na*] of 9000 $cm^{-3}$, corresponding the background, clean, and polluted atmosphere, respectively. In Cu-TP and Cu-NCP, the CWC achieves the highest under the high [*Na*] case and the lowest under the very low [*Na*] case (Figures 4a and 4b). A higher [*Na*] enhances CDNC and reduces $R_{eff}$, suppressing the conversion from cloud water to rain water and sustaining more CWC in the cloud. In Table 1, the initial formation time of rain water is delayed with the [*Na*]

Atmos. Chem. Phys. Discuss., doi:10.5194/acp-2017-148, 2017
Manuscript under review for journal Atmos. Chem. Phys.
Discussion started: 23 February 2017




211 increase in Cu-TP and Cu-NCP. The height of the maximum CWC slightly increases from
212 the very low to high [*Na*] conditions in Cu-TP and Cu-NTP, but the maximum CWC occurs
213 at 6~8 km a.s.l. in Cu-TP and 2~4 km a.s.l. in Cu-NCP. Therefore, for Cu-TP, most of cloud
214 droplets are above the 0°C isotherm (about 5 km a.s.l.) and supercooled.

215 The ice particles (ice + snow) generally attain the highest in the high [*Na*] and lowest in
216 the very low [*Na*], which is consistent with those of the CWC in Cu-TP and Cu-NCP (Figures
217 4e and 4f). In the present study, the homogeneous freezing and rime-splintering mechanisms
218 (DeMott et al., 1994; Hallett and Mossop, 1974) are included for the ice nucleation. In
219 addition, the heterogeneous ice nucleation, including the contact, immersion, and
220 condensation freezing, is parameterized using the method proposed by Philips et al. (2008;
221 2013), and has considered the IN effect, depending not only on temperature and ice
222 supersaturation, but also on the chemistry and surface area of multiple species of IN aerosols.
223 The [*Na*] Enhancement generally suppresses the warm rain process to reduce the rain water,
224 but provides more IN and supercooled CWC to accelerate the ice nucleation process. In
225 addition, the rime-splintering mechanism also affects the ice particle profiles at the height
226 with temperature ranging from -8°C and -3°C (Hallet and Mosssop, 1974). At the height of
227 6~8 km a.s.l. in Cu-TP and 4~6 km a.s.l. in Cu-NCP, the ice particles profiles are almost the
228 same in the very low and low [*Na*] cases, which is caused by the rime-splintering mechanism.
229 The ice crystal production from the rime-splintering mechanism is related to the graupel
230 particles and the cloud droplets with radii exceeding 24 $\mu m$. Large cloud droplets in the very
231 low [*Na*] facilitate the ice crystal productions from the rime-splintering mechanism,
232 increasing the ice particles mass concentrations at the height of 6~8 km a.s.l. in Cu-TP and
233 4~6 km a.s.l. in Cu-NCP. Furthermore, there are more ice particles in Cu-TP than Cu-NCP
234 with the same [*Na*] condition. The initial formation time of ice crystals is advanced by at least
235 12 minutes in Cu-TP compared to Cu-NCP (Table 1). The early formation of ice crystals not

Atmos. Chem. Phys. Discuss., doi:10.5194/acp-2017-148, 2017
Manuscript under review for journal Atmos. Chem. Phys.
Discussion started: 23 February 2017




only facilitates their growth, also advances the glaciation process to intensify convections, further enhancing the growth process.

The rainwater in Cu-TP achieves the highest in the very low [*Na*] and lowest in the high [*Na*], and vice versa in Cu-NCP (Figures 4c and 4d). If not considering the contribution of graupel melting to the rainwater, enhancement of [*Na*] suppresses the warm rain process to reduce the rainwater, but enhances the raindrop size, which conversely accelerates the raindrop falling (Table 1). In Cu-TP, due to relatively low temperature below the freezing level and short falling distance (about 1 km), graupels dominate the precipitating particles, melting less to rainwater. So early occurrence of the warm rain process in the very low [*Na*] case causes the most rainwater formation (Figure 4c). However, in Cu-NCP, graupels falling below the freezing level tend to melt due to high temperature and long falling distance (about 4 ~ 5 km), enhancing the rainwater formation. More ice particles and supercooled CWC in the high [*Na*] case are favorable for the ice growth through deposition, aggregation among ice crystals, and riming of supercooled droplets (Wang and Change, 1993a, b; Lou et al., 2003), and heavily rimed ice crystals are transferred to graupels, enhancing the graupel formation. Therefore, in Cu-NCP, the high [*Na*] corresponds to the maximum graupel content and also rainwater content (Figures 4d and 4h). However, in Cu-TP, below 12 km, the low [*Na*] corresponds to the largest amounts of graupels. Early occurrence of the glaciation process in Cu-TP causes most of raindrops to be frozen to form graupels. The freezing rate of raindrops depends on the temperature, the raindrop size and number, and their corresponding variations with time (Lou et al., 2003). Generally, the raindrops with the larger size are easier to be frozen under the lower temperature. The [*Na*] Enhancement decreases the raindrop number, but increases its size and updraft to lower the temperature, causing the maximum raindrop freezing efficiency under the low [*Na*] condition.

Atmos. Chem. Phys. Discuss., doi:10.5194/acp-2017-148, 2017
Manuscript under review for journal Atmos. Chem. Phys.
Discussion started: 23 February 2017




It is worth noting that ice particles and graupels are transported above 12 km a.s.l. or even exceeding 16 km a.s.l. (near tropopause) in Cu-TP, showing intensified convection and also contributing to moistening the upper troposphere.

### 3.2 Response of Convective Strength to Changes in Aerosol Concentrations

The p-mean of the updraft and downdraft in a core area is used to measure the convective strength of the simulated cumulus clouds, which is defined by the absolute vertical wind speed exceeding 1 m $s^{-1}$ and total condensed water mixing ratio more than $10^{-2}$ g $kg^{-1}$ (*Wang*, 2005). When the [*Na*] increases from 20 to 9000 $cm^{-3}$, the p-mean of the core updraft increases from 2.0 to 4.3 m $s^{-1}$ in Cu-TP, and from 1.5 to 2.7 m $s^{-1}$ in Cu-NCP (Figure 5a). The enhancement of the core updraft with increasing [*Na*] is caused by the suppression of the warm rain process to induce the more efficient mixed phase process, releasing more latent heat to intensify the convection. With the same [*Na*], the p-mean of the core updraft is larger in Cu-TP than in Cu-NCP, showing the significant impact of the early occurrence of the glaciation process on the cloud development.

In Cu-TP, with the [*Na*] increase, the p-mean of the downdraft increases when the [*Na*] is less than 90 $cm^{-3}$, but it becomes insensitive to the changes in [*Na*] when the [*Na*] is between 90 and 1800 $cm^{-3}$, and commences to decrease when the [*Na*] exceeds 1800 $cm^{-3}$ (Figure 5b). The complex nonlinear variation of the p-mean of the downdraft with the [*Na*] reflects the change in the vertical distribution of ice particles and graupels caused by the enhancement of [*Na*] in Cu-TP. The enhancement of the convective strength with increasing [*Na*] not only intensifies the convection to facilitate precipitation, producing more precipitable particles, but also transports more ice particles and graupels to the upper troposphere due to the specific topography and further suppress the occurrence of the downdraft. However, the p-mean of the downdraft in Cu-NCP increases steadily with [*Na*]. Such an increase in the core downdraft with [*Na*] might be caused by the formation of a large



mass loading of precipitable particles to reduce buoyancy and increase downdrafts. Interestingly, when the [*Na*] is less than about 450 $cm^{-3}$, the p-mean of downdraft in Cu-TP is greater than that in Cu-NCP, but opposite when [*Na*] exceeding 450 $cm^{-3}$, indicating the influence of the early occurrence of the glaciation process due to the specific topography in Cu-TP.

The maximum updraft, representing the largest local latent heat release, generally increases with [*Na*] in Cu-TP and Cu-NCP (Figure 6a). The maximum updraft in Cu-TP is much higher than that in Cu-NCP with the same [*Na*]. In Cu-TP, when the [*Na*] exceeds 750 $cm^{-3}$, the maximum updraft becomes insensitive to changes in the [*Na*]. In Cu-NCP, the maximum updraft is not very sensitive to changes in the [*Na*] when the [*Na*] exceeds 2400 $cm^{-3}$. The maximum downdraft, or the largest drag speed, indicating the largest strength to inhibit the development of the convection, also increases generally with the [*Na*] in Cu-TP and Cu-NCP (Figure 6b), but Cu-TP produces the more intensive maximum downdraft than Cu-NCP.

### 3.3 Response of Precipitation to Changes in Aerosol Concentrations

Figure 7 shows the variation of the accumulated precipitation with [*Na*] in Cu-TP and Cu-NCP. Generally, the precipitation increases with [*Na*], which is consistent with previous modeling studies (e.g., Khain et al., 2005, 2008; Fan et al., 2007; Li et al., 2008a; 2009). Since Cu-TP and Cu-NCP occur under humid conditions, the precipitation enhancement with [*Na*] is also in good agreement with measurements. Observations have shown the precipitation enhancement around heavily polluted coastal urban areas (Shepherd and Burian, 2003; Ohashi and kida, 2002) or over oceans influenced by pollution aerosols (Cerveny and Balling, 1998; Li et al., 2008b; Koren et al., 2012, 2014).

When the [*Na*] is increased from about 20 $cm^{-3}$ to 9000 $cm^{-3}$, the precipitation of Cu-TP increases from 0.13 mm to 0.23 mm; when the [*Na*] exceeds 300 $cm^{-3}$, the



precipitation becomes insensitive to the variation in [*Na*]. In contrast, the precipitation of Cu-NCP consistently increases from 0.03 mm to 0.37 mm with [*Na*] ranging from 20 $cm^{-3}$ to 9000 $cm^{-3}$. In addition, when the [*Na*] is less than 500 $cm^{-3}$, Cu-TP produces more precipitation than Cu-NCP, which can be explained by the early occurrence of the glaciation process causing less warm rain but more efficient mixed-phase processes. However, when the [*Na*] exceeds 500 $cm^{-3}$, the precipitation efficiency of Cu-NCP is higher than that of Cu-TP, although the convective strength is larger in Cu-TP than Cu-NCP. The increasing convective strength with [*Na*] not only enhances the precipitation, but also transports more ice particles and graupels above 12 km to form the anvil. The ice particles and grauples in the anvil are subject to sublimation and evaporation to moisten the upper troposphere, and decrease the precipitation efficiency in Cu-TP.

### 3.4 Sensitivity Studies

Recent studies have demonstrated that convections are active and strong during summertime over Tibetan Plateau due to its unique thermodynamic forcing (Hu et al., 2016). We have further performed sensitivity studies to explore the impact of the maximum perturbation temperature (MPT) in the warm bubble on the development of cumulus clouds. The MPTs of 2.0°C and 0.5°C are used to trigger Cu-TP and Cu-NCP with the [*Na*] ranging from 20 $cm^{-3}$ to 9000 $cm^{-3}$.

For Cu-TP, the core updraft decreases slightly when the MPT is reduced from 4.0°C to 2.0°C, particularly when the [*Na*] exceeds 100 $cm^{-3}$, the decrease of the core updraft is indiscernible. When the MPT is reduced from 2.0°C to 0.5°C, the core updraft decreases considerably. However, for Cu-NCP, the core updraft decreases substantially when the MPT is reduced from 4.0°C to 0.5°C. When the MPT is 0.5°C and the [*Na*] is less than 80 $cm^{-3}$, the updraft core area is not formed in Cu-NCP. When the MPT is the same, the core updraft is much larger in Cu-TP than Cu-NCP with the same [*Na*]; even the core updraft in Cu-TP with



335 the MPT of 0.5°C is larger than that in Cu-NCP with the MPT of 4.0°C when the [*Na*] is
336 more than 80 $cm^{-3}$. Therefore, under the unstable conditions over the Tibetan Plateau, a small
337 perturbation can induce strong convections, which is primarily caused by early occurrence of
338 the glaciation process due to the specific topography, as discussed in Section 3.1.

339 The accumulated precipitation generally decreases with the MPT in Cu-TP and
340 Cu-NCP with the same [*Na*]. When the MPT is 4.0°C, Cu-NCP produces more precipitation
341 than Cu-TP with the [*Na*] exceeding 500 $cm^{-3}$, but Cu-TP produces much more precipitation
342 than Cu-NCP with the MPT of 0.5°C under all aerosol conditions. In addition, the
343 precipitation generally increases with increasing the [*Na*] in Cu-TP and Cu-NCP with various
344 MPTs, and does not exhibit a nonlinear variation with the [*Na*], which is not consistent with
345 the results in Li et al. (2008a). The possible reason is that in this study, the maximum p-mean
346 of CDNC is about 410 $cm^{-3}$, which is much less than that in Li et al. (2008a). If further
347 increasing the [*Na*], the precipitation might be suppressed.
348

349 **4. Summary and Conclusions**

350 The aerosol-cloud interaction over the TP has been examined using the CR-WRF
351 model with a two moment microphysical scheme considering the aerosol effects on CCN and
352 IN. For comparisons, two types of cumulus clouds, occurring over the TP and NCP in August
353 2014, are modeled to examine the response of the cumulus clouds development to the change
354 in aerosol concentrations. A set of 28 aerosol profiles are utilized in simulations, with the
355 surface aerosol number concentration varying from 20 to 9000 $cm^{-3}$ and the sulfate mass
356 concentration varying from 0.02 to 9.0 μg $cm^{-3}$. Multiple aerosol species are considered to
357 provide CCN and IN, including sulfate, nitrate, ammonium, organic and black carbon, and
358 dust-like aerosols.



359 In general, with varying aerosol concentrations from very clean background condition
360 to the polluted condition, more aerosols are activated, significantly increasing the CDNC and
361 decreasing the droplet size in Cu-TP and Cu-NCP. Formation of a large amount of cloud
362 droplets with small sizes suppresses the warm rain process and enhances water vapor
363 condensation efficiency and updraft to generate more available condensable water vapor.
364 When more cloud droplets are transported above the 0°C isotherm, occurrence of the
365 mixed-phase process releases more latent heat to further enhance the cloud core updraft and
366 increase precipitation, intensifying the convections in Cu-TP and Cu-NCP.

367 However, early occurrence of the glaciation process in Cu-TP, which is triggered at an
368 elevation of more than 4000 m, causes large differences between Cu-TP and Cu-NCP. Much
369 more supercooled cloud droplets are formed in Cu-TP than Cu-NCP with the same aerosol
370 concentration, facilitating the mixed-phase process and significantly enhancing the core
371 updraft and maximum updraft in Cu-TP compared to Cu-NCP. Nevertheless, the intensified
372 convection induced by the increase of aerosol concentrations in Cu-TP not only facilitates the
373 precipitation, but also delivers more ice-phase hydrometeors into the upper troposphere to
374 form the anvil, decreasing the precipitation efficiency. Therefore, in Cu-TP, when aerosol
375 concentrations are high, the precipitation enhancement becomes insignificant with increasing
376 aerosol concentrations, but a considerable amount of ice-phase hydrometeors are lofted above
377 12 km or even exceeding 16 km. Additionally, sensitivity studies have also shown that under
378 the unstable conditions over the TP, a small perturbation in temperature can induce strong
379 convections, which is primarily caused by early occurrence of the glaciation process due to
380 the specific topography.

381 Rapid growth of industrialization, urbanization, and transportation in Asia has caused
382 severe air pollution, progressively increasing aerosol concentrations in the regions
383 surrounding TP. Pollution aerosols from surrounding areas have been observed to be



transported to the TP. Considering the very clean atmosphere over the TP, elevated aerosol concentrations can considerably enhance the convections due to its specific topography. Numerous studies have shown that the TP significantly influences the formation and variability of the Asian summer monsoon through mechanical and thermal dynamical effects (e.g., Wu et al., 2007). In addition, Fu et al. (2006) have reported that convection over the TP provides the main pathway for cross-tropopause transport in the Asian monsoon/TP region. Hence, intensification of convections due to the increase of aerosol concentrations over the TP not only enhances the latent heat release to warm the middle troposphere, influencing the Asian summer monsoon, also delivers more hydrometeors into the upper troposphere, allowing more water vapor to travel into the lower stratosphere. Further studies are needed to evaluate the aerosol indirect effect on the Asian summer monsoon and the troposphere/stratosphere exchange over the TP.

*Acknowledgements.* This work was supported by the National Natural Science Foundation of China (No. 41275153) and by the "Hundred Talents Program" of the Chinese Academy of Sciences. Naifang Bei is supported by the National Natural Science Foundation of China (No. 41275101). Luisa Molina and Wenfang Lei acknowledge support from US NSF Award 1560494.



403 **Reference**

404 Ackerman, T. P.: A model of the effect of aerosols on urban climates with particular
405 applications to the Los Angeles basin, J. Atmos. Sci., 34(3), 531–547, 1977.

406 Albrecht, B. A.: Aerosols, cloud microphysics, and fractional cloudiness, Science, 245,
407 1227–1230, doi:10.1126/science.245.4923.1227, 1989.

408 Andreae, M. O., Rosenfeld, D., Artaxo, P., Costa, A. A., Frank, G. P., Longo, K. M., and
409 Silva-Dias, M. A. F.: Smoking rain clouds over the Amazon, Science, 303, 1337–1342,
410 2004.

411 Binkowski, F. S. and Roselle, S. J.: Models-3 Community Multiscale Air Quality (CMAQ)
412 model aerosol component 1. Model description, J. Geophys. Res., 108, 4183,
413 doi:10.1029/2001JD001409, 2003.

414 Cerveny, R. S. and Bailing Jr., R. C.: Weekly cycles of air pollutants, precipitation and
415 tropical cyclones in the coastal NW Atlantic region, Nature, 394, 561–563, 1998.

416 Dagan, G., Koren, I., and Altaratz, O.: Aerosol effects on the timing of warm rain processes,
417 Geophys. Res. Lett., 42, 4590–4598, doi:10.1002/2015GL063839, 2015.

418 Decesari, S., Facchini, M. C., Carbone, C., Giulianelli, L., Rinaldi, M., Finessi, E., Fuzzi, S.,
419 Marinoni, A., Cristofanelli, P., Duchi, R., Bonasoni, P., Vuillermoz, E., Cozic, J., Jaffrezo,
420 J. L., and Laj, P.: Chemical composition of $PM_{10}$ and $PM_1$ at the high-altitude Himalayan
421 station Nepal Climate Observatory-Pyramid (NCO-P) (5079 m a.s.l.), Atmos. Chem.
422 Phys., 10, 4583–4596, doi:10.5194/acp-10-4583-2010, 2010.

423 DeMott, P. J., Meyers, M. P., and Cotton, W. R.: Parameterization and impact of ice
424 initiation processes relevant to numerical model simulations of cirrus clouds, J. Atmos.
425 Sci., 51, 77–90, doi:10.1175/1520-0469(1994)051<0077:paioii> 2.0.co;2, 1994.

426 D'Errico, M., Cagnazzo, C., Gogli, P. G., Lau, K. M., Von, H. J., Fierli, F., and Cherchi, A.:
427 Indian monsoon and the elevated-heat pump mechanism in a coupled aerosol-climate
428 model, J. Geophys. Res., 120, 8712–8723, doi: 10.1002/2015JD023346, 2015.

429 Ding, Y. H., Wang, Z. Y., and Sun, Y.: Inter-decadal variation of the summer precipitation in
430 East China and its association with decreasing Asian summer monsoon. Part I: observed
431 evidences, Int. J. Climatol., 28, 1139–1161, doi: 10.1002/joc.1615, 2008.

432 Engling, G., Zhang, Y.-N., Chan, C.-Y., Sang, X.-F., Lin, M., Ho, K.-F., Li, Y.-S., Lin, C.-Y.,
433 and Lee, J. J.: Characterization and sources of aerosol particles over the southeastern
434 Tibetan Plateau during the Southeast Asia biomass-burning season, Tellus B, 63, 117–
435 128, doi:10.1111/j.1600-0889.2010.00512.x, 2011.

436 Fan, J. W., Leung, L. R., Rosenfeld, D., Chen, Q., Li, Z. Q., Zhang, J. Q., and Yan, H. R.:
437 Microphysical effects determine macrophysical response for aerosol impacts on deep
438 convective clouds, P. Natl. Acad. Sci. USA, 110, E4581–E4590,
439 doi:10.1073/pnas.1316830110, 2013.

440 Fan, J. W., Yuan, T. L., Comstock, J. M., Ghan, S., Khain, A., Leung, L. R., Li, Z. Q.,
441 Martins, V. J., and Ovchinnikov, M.: Dominant role by vertical wind shear in regulating
442 aerosol effects on deep convective clouds, J. Geophys. Res., 114, D22206,
443 doi:10.1029/2009jd012352, 2009.

444 Fan, J., Zhang, R., Li, G., Tao, W.-K and Li, X.: Simulations of cumulus clouds using a
445 spectral microphysics cloud-resolving model, J. Geophys. Res., 112, D04201,
446 doi:10.1029/2006JD007688, 2007a.



447 Fan, J., Zhang, R., Li, G., and Tao, W.-K.: Effects of aerosols and relative humidity on
448 cumulus clouds, J. Geophys. Res., 112, D14204, doi:10.1029/2006JD008136, 2007b.

449 Fu, R., Hu, Y., Wright, J. S., Jiang, J. H., Dickinson, R. E., Chen, M., Filipiak, M., Read, W.
450 G., Waters, J. W., and Wu, D. L.: Short circuit of water vapor and polluted air to the
451 global stratosphere by convective transport over the Tibetan Plateau, P. Natl. Acad. Sci.
452 USA, 103, 5664–5669, doi:10.1073/pnas.0601584103, 2006.

453 Hallett, J. and Mossop, S. C.: Production of secondary ice crystals during the riming process,
454 Nature, 249, 26–28, 1974.

455 Hobbs, P. V.: Aerosol-cloud-climate interactions (Vol. 54), Academic Press, 1993.

456 Houghton J.: The science of global warming, Interdiscip. Sci. Rev., 26, 247–257,
457 doi:10.1179/030801801679485, 2001.

458 Hu, L., Deng, D., Gao, S., and Xu, X.: The seasonal variation of Tibetan Convective Systems:
459 Satellite observation, J. Geophys. Res., 121, doi:10.1002/2015JD024390, 5512–5525,
460 2016.

461 IPCC: Summary for Policymakers, in: Climate Change 2013: The Physical Science Basis.
462 Contribution of Working Group I to the Fifth Assessment Report of the
463 Intergovernmental Panel on Climate Change, edited by: Stocker, T. F., Qin, D., Plattner,
464 G.-K., Tignor, M., Allen, S. K., Boschung, J., Nauels, A., Xia, Y., Bex, V., and Midgley,
465 P. M., Cambridge University Press, Cambridge, UK and New York, NY, USA, 2013.

466 Jacobson, M. Z.: Analysis of aerosol interactions with numerical techniques for solving
467 coagulation, nucleation, condensation, dissolution, and reversible chemistry among
468 multiple size distributions, J. Geophys. Res., 107, 4366, doi:10.1029/2001JD002044,
469 2002.

470 Kaufman, Y. J. and Nakajima, T.: Effect of Amazon smoke on cloud microphysics and
471 albedo – Analysis from satellite imagery, J. Appl. Meteor., 32, 729–744, 1993.

472 Kaufman, Y. J., Koren, I., Remer, L. A., Rosenfeld, D., and Rudich, Y.: The effect of smoke,
473 dust, and pollution aerosol on shallow cloud development over the Atlantic Ocean, P.
474 Natl. Acad. Sci. USA, 102, 11207–11212, doi:10.1073/pnas.0505191102, 2005.

475 Khain, A. P.: Notes on state-of-art investigations of aerosol effects on precipitation: a critical
476 review, Environ. Res. Lett., 4, 015004, doi:10.1088/1748-9326/4/1/015004, 2000.

477 Khain, A. P., BenMoshe, N., and Pokrovsky, A.: Factors determining the impact of aerosols
478 on surface precipitation from clouds: An attempt at classification, J. Atmos. Sci., 65,
479 1721–1748, doi:10.1175/2007jas2515.1, 2008.

480 Khain, A., Rosenfeld, D., and Pokrovsky, A.: Aerosol impact on the dynamics and
481 microphysics of deep convective clouds, Q. J. Roy. Meteor. Soc., 131, 2639–2663,
482 doi:10.1256/Qj.04.62, 2005.

483 Koren, I., Altaratz, O., Remer, L. A., Feingold, G., Martins, J. V., and Heiblum, R. H.:
484 Aerosol-induced intensification of rain from the tropics to the mid-latitudes, Nat. Geosci.,
485 5, 118–122, doi:10.1038/NGEO1364, 2012.

486 Koren, I., Dagan, G., and Altaratz, O.: From aerosol-limited to invigoration of warm
487 convective clouds, Science, 344, 1143–1146, doi:10.1126/science.1252595, 2014.

488 Koren, I., Remer, L. A., Altaratz, O., Martins, J. V., and Davidi, A.: Aerosol-induced changes
489 of convective cloud anvils produce strong climate warming, Atmos. Chem. Phys., 10,
490 5001–5010, doi:10.5194/acp-10-5001-2010, 2010.



491 Lau, K.-M., Tsay, S. C., Hsu, C., Chin, M., Ramanathan, V., Wu, G.-X., Li, Z., Sikka, R.,
492 Holben, B., Lu, D., Chen, H., Tartari, G., Koudelova, P., Ma, Y., Huang, J., Taniguchi, K.,
493 and Zhang, R.: The joint aerosol-monsoon experiment: A new challenge for Monsoon
494 Climate Research, B. Am. Meteorol. Soc., 89, 369–383, 2008.

495 Lee, S. S., Donner, L. J., Phillips, V. T. J., and Ming, Y.: The dependence of aerosol effects
496 on clouds and precipitation on cloud-system organization, shear and stability, J. Geophys.
497 Res., 113, D16202, doi:10.1029/2007jd009224, 2008.

498 Levin, Z. and Cotton, W.: Aerosol pollution impact on precipitation: A scientific review,
499 World Meteorological Organization, Geneva, Switzerland, 2007.

500 Li, G. H., Wang, Y., and Zhang, R. Y.: Implementation of a two- moment bulk microphysics
501 scheme to the WRF model to investigate aerosol-cloud interaction, J. Geophys. Res., 113,
502 D15211, doi:10.1029/2007jd009361, 2008a.

503 Li, G., Wang, Y., Lee, K.-H., Diao, Y., and Zhang, R.: Increased winter precipitation over the
504 North Pacific from 1984 – 1994 to 1995 – 2005 inferred from the Global Precipitation
505 Climatology Project, Geophys. Res. Lett., 35, L13821, doi:10.1029/2008GL034668,
506 2008b.

507 Li, G., Wang, Y., Lee, K.-H., Diao, Y., and Zhang, R.: Impacts of aerosols on the
508 development and precipitation of a mesoscale squall line, J. Geophys. Res., 114, D17205,
509 doi:10.1029/2008JD011581, 2009.

510 Li, L., Hong, Y., Wang, J., Adler, R. F., Pollcelli, F. S., Habib, S., Irwn, D., Korme, T., and
511 Okello, L.: Evaluation of the real-time TRMM-based multi-satellite precipitation analysis
512 for an operational flood prediction system in Nzoia Basin, Lake Victoria, Africa, Nat.
513 Hazards, 50, 109, doi:10.1007/s11069-008-9324-5, 2009.

514 Li, X., Tao, W.-K., Masunaga, H., Gu, G., and Zeng , X.: Aerosol effects on cumulus
515 congestus population over the tropical Pacific: Cloud resolving modeling study, J.
516 Meteorol. Soc. Jpn., 91, 817–833, 2013.

517 Loftus, A.M., and Cotton, W.R.: Examination of CCN impacts on hail in a simulated
518 supercell storm with triple-moment hail bulk microphysics, Atmos. Res., s147–148(1),
519 183–204, 2014.

520 Lou, X.-F., Hu, Z.-J., and Shi, Y.-Q.: Numerical simulation of a heavy rainfall case in South
521 China, Adv. Atmos. Sci., 20, 128–138, 2003.

522 McComiskey, A. and Feingold, G.: The scale problem in quantifying aerosol indirect effects,
523 Atmos. Chem. Phys., 12, 1031-1049, doi:10.5194/acp-12-1031-2012, 2012.

524 Ohashi, Y. and Kida, H.: Local circulations developed in the vicinity of both coastal and
525 inland urban areas: A numerical study with a mesoscale atmospheric model, J. Appl.
526 Meteor., 41(1), 30–45, 2002.

527 Penner, J. E., Hegg, D., and Leaitch, R.: Unraveling the role of aerosols in climate change,
528 Environ. Sci. Technol., 35, 332–340, 2001.

529 Petters, M. D. and Kreidenweis, S. M.: A single parameter representation of hygroscopic
530 growth and cloud condensation nucleus activity, Atmos. Chem. Phys., 7, 1961–1971,
531 doi:10.5194/acp-7-1961-2007, 2007.

532 Petters, M. D. and Kreidenweis, S. M.: A single parameter representation of hygroscopic
533 growth and cloud condensation nucleus activity – Part 2: Including solubility, Atmos.
534 Chem. Phys., 8, 6273–6279, doi:10.5194/acp-8-6273-2008, 2008.



535 Petters, M. D. and Kreidenweis, S. M.: A single parameter representation of hygroscopic
536 growth and cloud condensation nucleus activity – Part 3: Including surfactant partitioning,
537 Atmos. Chem. Phys., 13, 1081–1091, doi:10.5194/acp-13-1081-2013, 2013.

538 Phillips, T. J., DeMott, P. J., and Andronache, C.: An empirical parameterization of
539 heterogeneous ice nucleation for multiple chemical species of aerosol, J. Atmos. Sci., 65,
540 2757–2783, 2008.

541 Phillips, T. J., DeMott, P. J., Andronache, C., Pratt, K. A., Prather, K. A., Subramanian, R.,
542 and Twohy, C.: Improvements to an empirical parameterization of heterogeneous ice
543 nucleation and its comparison with observations, 70, 378–408, 2013.

544 Pruppacher, H. R. and Klett, J. D.: Microphysics of clouds and precipitation, second revised
545 and enlarged edition with an introduction to cloud chemistry and cloud electricity,
546 Kluwer Academic Publishers, Reidel, Dordrecht, 954 pp., 1997.

547 Ramanathan. V., Crutzen, P. J., Kiehl, J. T., and Rosenfeld, D.: Aerosols, climate, and the
548 hydrological cycle, Science, 294, 2119–2124, 2001.

549 Rogers, R. R. and Yau, M. K.: A short course in cloud physics, Pergamon, Tarrytown, New
550 York, 1989.

551 Rosenfeld, D.: Suppression of rain and snow by urban and industrial air pollution, Science,
552 287, 1793–1796, 2000.

553 Rosenfeld, D. and Lensky, I. M.: Satellite-based insights into precipitation formation
554 processes in continental and maritime convective clouds, B. Am. Meteorol. Soc., 79,
555 2457–2476, 1998.

556 Rosenfeld, D., and Woodley, W. L.: Deep convective clouds with sustained supercooled
557 liquid water down to -37.5 C, Nature, 405, 440–442, 2000.

558 Rosenfeld, D., Lohmann, U., Raga, G. B., O'Dowd, C. D., Kulmala, M., Fuzzi, S., Reissell,
559 A., and Andreae, M. O.: Flood or drought: how do aerosols affect precipitation?, Science,
560 321, 1309–1313, 2008.

561 Shepherd, J. M., and Burian, S. J.: Detection of urban-induced rainfall anomalies in a major
562 coastal city, Earth Interact., 7, 1–14,
563 doi:10.1175/1087-3562(2003)007<0001:DOUIRA>2.0.CO;2, 2003.

564 Skamarock, W. C.: Evaluating mesoscale NWP models using kinetic energy spectra, Mon.
565 Weather Rev., 132, 3019–3032, 2004.

566 Tao, W. K., Li, X. W., Khain, A., Matsui, T., Lang, S., and Simpson, J.: Role of atmospheric
567 aerosol concentration on deep convective precipitation: Cloud-resolving model
568 simulations, J. Geophys. Res., 112, D24S18, doi:10.1029/2007jd008728, 2007.

569 Twomey, S. A.: The influence of pollution on the shortwave albedo of clouds, J. Atmos. Sci.,
570 34, 1149–1152, 1977.

571 Van Den Heever, S. C. and Cotton, W. R.: Urban aerosol impacts on downwind convective
572 storms, J. Appl. Meteorol. Clim., 46, 828–850, doi:10.1175/JAM2492.1, 2007.

573 Wang, C. and Chang, J.: Three-dimensional numerical model of cloud dynamics,
574 microphysics, and chemistry 1. Concepts and formulation, J. Geophys. Res., 98(D8), 14
575 827–14 844, 1993a.



576 Wang, C. and Chang, J.: Three-dimensional numerical model of cloud dynamics,
577 microphysics, and chemistry 2. A case study of the dynamics and microphysics of a
578 severe local storm, J. Geophys. Res., 98(D8), 14,845–14,862, 1993b.

579 Wang, C.: A modeling study of the response of tropical deep convection to the increase of
580 cloud condensation nuclei concentration, 1. Dynamics and microphysics, J. Geophys.
581 Res., 110, D21211, doi:10.1029/2004JD005720, 2005.

582 Wu, G., Liu, Y., Zhang, Q., Duan, A., Wang, T., Wan, R., Liu, X., Li, W., Wang, Z., and
583 Liang, X.: The influence of mechanical and thermal forcing by the Tibetan Plateau on
584 Asian climate, J. Hydrometeorol., 8, 770–789, doi:10.1175/JHM609.1, 2007.

585 Xu, B., Cao, J., Hansen, J., Yao, T., Joswia, D. R., Wang, N., Wu, G., Wang, M., Zhao, H.,
586 and Yang, W.: Black soot and the survival of Tibetan glaciers, P. Natl. Acad. Sci. USA,
587 106, 22114–22118, doi:10.1073/pnas.0910444106, 2009.

588 Yang, X., Ferrat, M. and Li, Z.: New evidence of orographic precipitation suppression by
589 aerosols in central China, Meteorol. Atmos. Phys., 119,17–29,
590 doi:10.1007/s00703-012-0221-9, 2013.

591 Zhang, R. Y., Li, G. H., Fan, J. W., Wu, D. L., and Molina, M. J.: Intensification of Pacific
592 storm track linked to Asian pollution, P. Natl. Acad. Sci. USA, 104, 5295–5299, 2007.

593

594

595

596

Atmos. Chem. Phys. Discuss., doi:10.5194/acp-2017-148, 2017
Manuscript under review for journal Atmos. Chem. Phys.
Discussion started: 23 February 2017


Atmospheric Chemistry and Physics Discussions

597 Table 1 Response of cloud properties in Cu-TP and Cu-NCP under three aerosol conditions*.
598

| Clouds | Cu-TP | | | Cu-NCP | | |
|---|---|---|---|---|---|---|
| | Background | Clean | Polluted | Background | Clean | Polluted |
| Initial formation time of hydrometeors (minutes) | | | | | | |
| Rain | 10 | 14 | 20 | 8 | 10 | 14 |
| Ice crystal | 12 | 10 | 8 | 24 | 24 | 26 |
| Graupel | 12 | 14 | 16 | 18 | 18 | 16 |
| P-mean of effective radius of hydrometeors (μm) | | | | | | |
| Rain | 119 | 132 | 647 | 110 | 151 | 223 |
| Graupel | 559 | 665 | 917 | 221 | 303 | 447 |

599
600 *The aerosol concentrations are 90, 900, and 9000 $cm^{-3}$ for the background, clean, and polluted conditions,
601 respectively.
602
603
604
605

Atmos. Chem. Phys. Discuss., doi:10.5194/acp-2017-148, 2017
Manuscript under review for journal Atmos. Chem. Phys.
Discussion started: 23 February 2017


Atmospheric Chemistry and Physics Discussions

## Figure Captions

Figure 1 Atmospheric sounding (a) over the Tibetan Plateau (87.08°E, 28.63°N, 4302 m a.s.l.) at 0800 UTC on August 12, 2014 and (b) over North China Plain (114.35°E, 37.17°N, 181 m a.s.l.) at 0800 UTC on August 24, 2014. The black line corresponds to the temperature, and the blue line represents the dew point temperature.

Figure 2 Modeled p-mean of (a) cloud droplet number concentration and (b) effective radius as a function of the initial [$N_a$] in Cu-TP and Cu-NCP.

Figure 3 Modeled p-mean of (a) cloud water mass concentration and (b) supercooled cloud water mass concentration as a function of the initial [$N_a$] in Cu-TP and Cu-NCP in Cu-TP and Cu-NCP.

Figure 4 Vertical profiles of time-averaged masses of hydrometeors under background (90 $cm^{-3}$, blue), clean (900 $cm^{-3}$, green), and polluted (9000 $cm^{-3}$, red) [$N_a$] for (a) and (b) cloud water, (c) and (d) rain water, (e) and (f) ice particles (ice + snow), and (g) and (h) graupel in Cu-TP and Cu-NCP, respectively.

Figure 5 Simulated p-mean of (a) updraft and (b) downdraft in the core area (defined as an area where the absolute vertical velocity of wind is greater than 1 m $s^{-1}$ and the total condensed water content exceeds $10^{-2}$ g $kg^{-1}$) as a function of the initial [$N_a$] in Cu-TP and Cu-NCP.

Figure 6 Modeled (a) maximum updraft and (b) minimum downdraft as a function of the initial [$N_a$] in Cu-TP and Cu-NCP.

Figure 7 Modeled cumulative precipitation inside the model domain (mm) as a function of the initial [$N_a$] in Cu-TP and Cu-NCP.

Figure 8 Response of (a) the p-mean of core updraft and (b) cumulative precipitation inside the model domain to the change in the maximum perturbation temperature of the warm bubble under various aerosol conditions in Cu-TP and Cu-NCP.

Atmos. Chem. Phys. Discuss., doi:10.5194/acp-2017-148, 2017
Manuscript under review for journal Atmos. Chem. Phys.
Discussion started: 23 February 2017


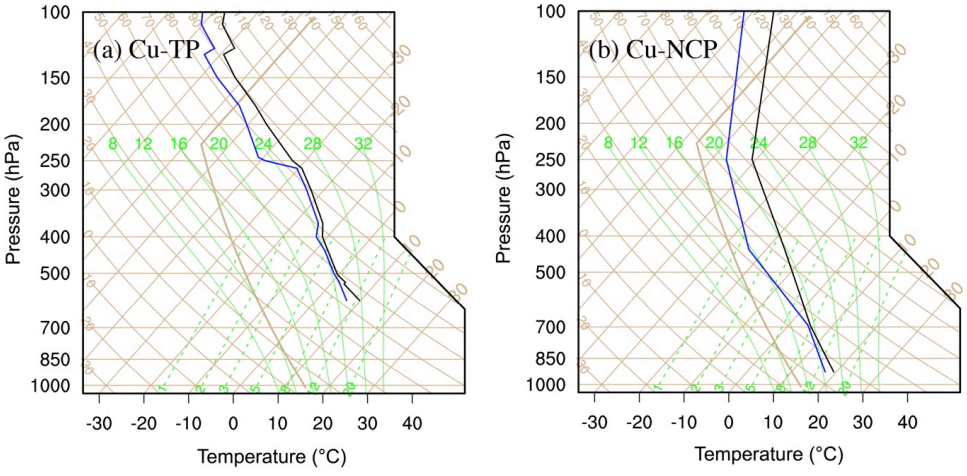


Figure 1 Atmospheric sounding (a) over the Tibetan Plateau (87.08°E, 28.63°N, 4302 m a.s.l.) at 0800 UTC on August 12, 2014 and (b) over North China Plain (114.35°E, 37.17°N, 181 m a.s.l.) at 0800 UTC on August 24, 2014. The black line corresponds to the temperature, and the blue line represents the dew point temperature.

Atmos. Chem. Phys. Discuss., doi:10.5194/acp-2017-148, 2017
Manuscript under review for journal Atmos. Chem. Phys.
Discussion started: 23 February 2017


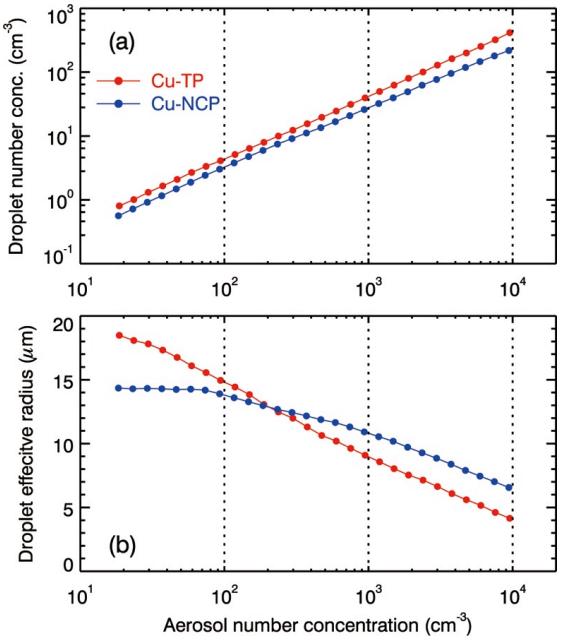


Figure 2 Modeled p-mean of (a) cloud droplet number concentration and (b) effective radius as a function of the initial [$N_a$] in Cu-TP and Cu-NCP.

Atmos. Chem. Phys. Discuss., doi:10.5194/acp-2017-148, 2017
Manuscript under review for journal Atmos. Chem. Phys.
Discussion started: 23 February 2017


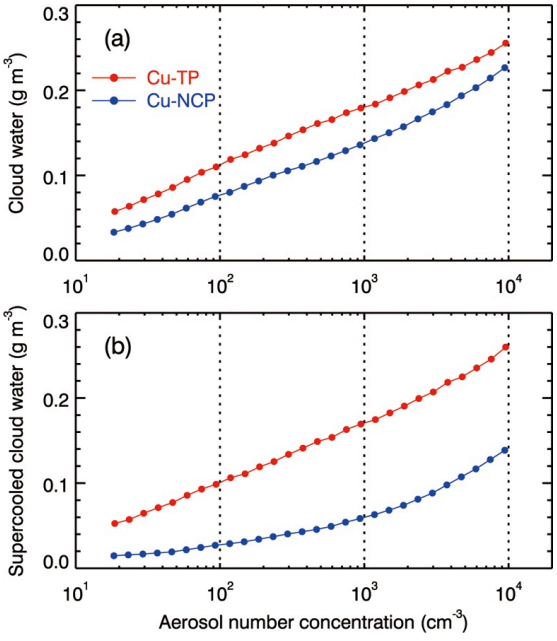


Figure 3 Modeled p-mean of (a) cloud water mass concentration and (b) supercooled cloud water mass concentration as a function of the initial [$N_a$] in Cu-TP and Cu-NCP in Cu-TP and Cu-NCP.

Atmos. Chem. Phys. Discuss., doi:10.5194/acp-2017-148, 2017
Manuscript under review for journal Atmos. Chem. Phys.
Discussion started: 23 February 2017


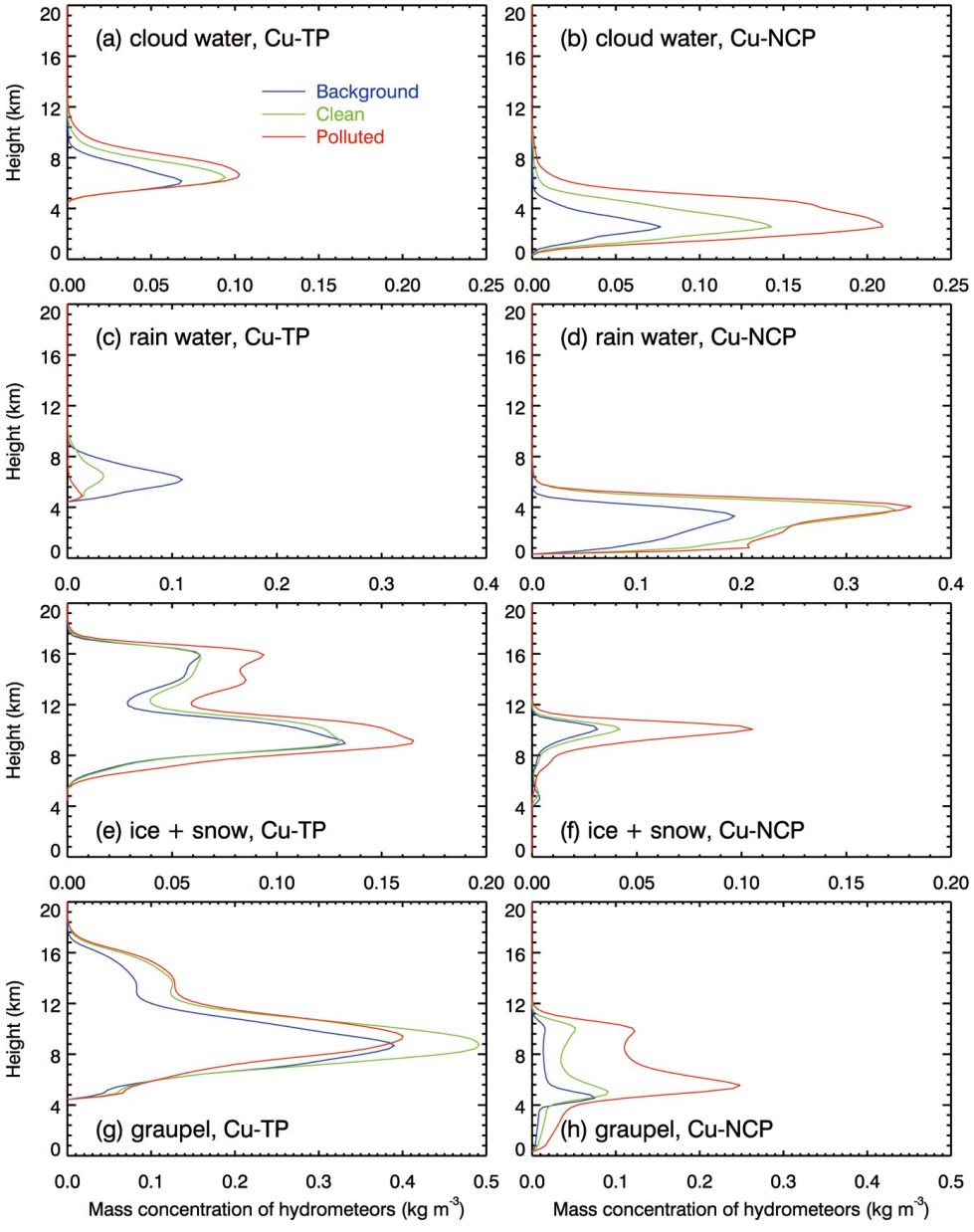


Figure 4 Vertical profiles of time-averaged masses of hydrometeors under background (90 $cm^{-3}$, blue), clean (900 $cm^{-3}$, green), and polluted (9000 $cm^{-3}$, red) [$N_a$] for (a) and (b) cloud water, (c) and (d) rain water, (e) and (f) ice particles (ice + snow), and (g) and (h) graupel in Cu-TP and Cu-NCP, respectively.

Atmos. Chem. Phys. Discuss., doi:10.5194/acp-2017-148, 2017
Manuscript under review for journal Atmos. Chem. Phys.
Discussion started: 23 February 2017


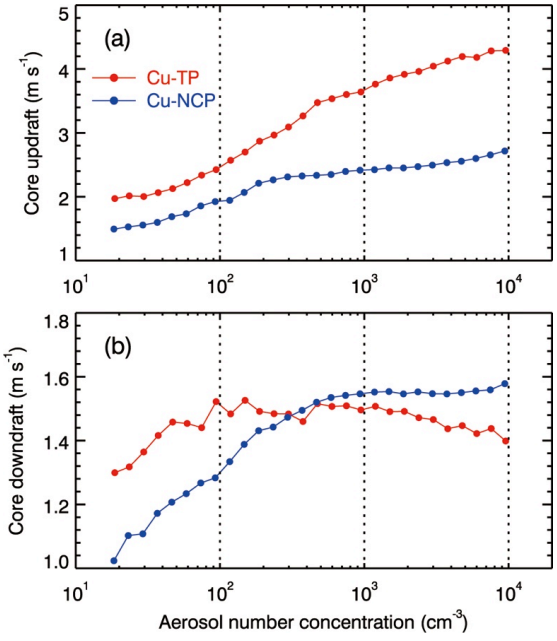


Figure 5 Simulated p-mean of (a) updraft and (b) downdraft in the core area (defined as an area where the absolute vertical velocity of wind is greater than 1 m $s^{-1}$ and the total condensed water content exceeds $10^{-2}$ g $kg^{-1}$) as a function of the initial [$N_a$] in Cu-TP and Cu-NCP.

Atmos. Chem. Phys. Discuss., doi:10.5194/acp-2017-148, 2017
Manuscript under review for journal Atmos. Chem. Phys.
Discussion started: 23 February 2017


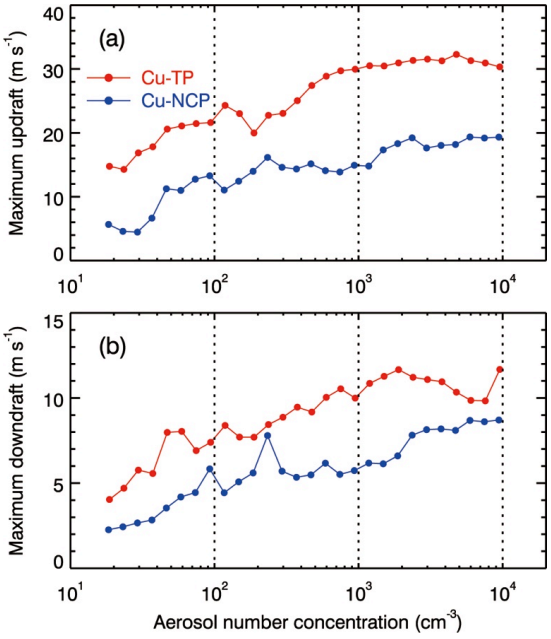


Figure 6 Modeled (a) maximum updraft and (b) minimum downdraft as a function of the initial [$N_a$] in Cu-TP and Cu-NCP.

Atmos. Chem. Phys. Discuss., doi:10.5194/acp-2017-148, 2017
Manuscript under review for journal Atmos. Chem. Phys.
Discussion started: 23 February 2017


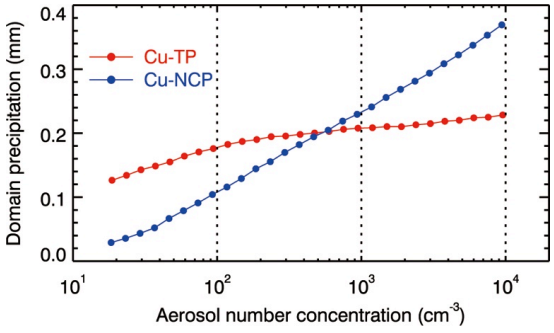


Figure 7 Modeled cumulative precipitation inside the model domain (mm) as a function of the initial [$N_a$] in Cu-TP and Cu-NCP.

Atmos. Chem. Phys. Discuss., doi:10.5194/acp-2017-148, 2017
Manuscript under review for journal Atmos. Chem. Phys.
Discussion started: 23 February 2017


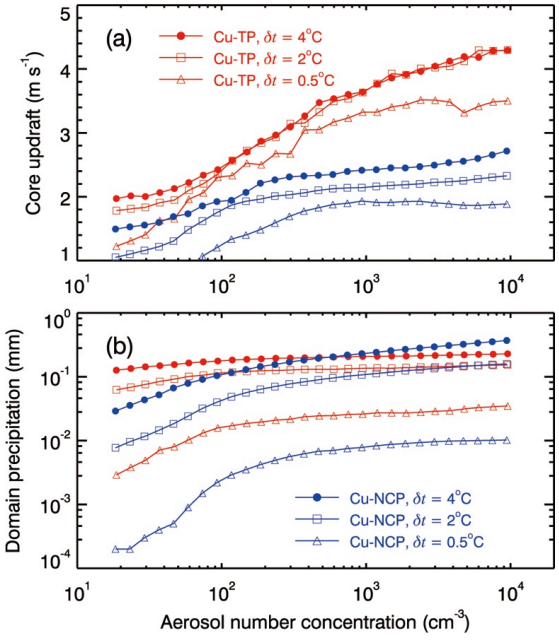


Figure 8 Response of (a) the p-mean of core updraft and (b) cumulative precipitation inside the model domain to the change in the maximum perturbation temperature of the warm bubble under various aerosol conditions in Cu-TP and Cu-NCP.